ASL Environmental Sciences Inc.
#1-6703 Rajpur Place
Saanichton, BC Canada V8M 1Z5
December 30, 2022
TECHNICAL REPORT

The interpretation of multi-frequency acoustic profiling; Part 2: a semi-empirical model of backscatter returns from frazil ice suspensions.

David R. Topham[1] and J.R. Marko[1]
[1]ASL Environmental Sciences Inc., Saanichton, BC, Canada
Correspondence: David R. Topham (dtopham@aslenv.com)

Abstract

A semi-empirical acoustic backscatter model representing a log-normal distributions of disk shaped frazil ice particles is developed to provide estimates of suspended fractional frazil volume. For three frequencies, the acoustic equations are fully determined and the solutions are numerically exact. The model defines conditions that must be satisfied for a given data set to support exact the solutions, allowing their existence to be established prior to analysis. Where more than three frequencies are available, inter-comparison of independent 3-frequency solutions provides error bounds on estimates of frazil fractional volumes. Examples drawn from both river and marine acoustic data sets provide estimates of frazil fractional volumes with typical error bounds of ±10%.

1. Introduction

Part 1 of this investigation (Topham, 2022), examines the general question of the conditions necessary for a three parameter acoustic backscatter model to support solutions for a given data set. This requires that pairs of ratios of volume backscatter coefficient data sharing a common frequency, satisfy a relationship between corresponding ratios defined by the theoretical model. Under these conditions, the equations of the algorithm are fully determined, and the solutions are "exact " in the sense that residuals of a search algorithm are vanishingly small, limited only by the numerical precision of the algorithm. The equations, expressed in terms of ratios of volume backscatter coefficients (Hay, and Sheng, 1992), are solved for the particle distribution parameters of particle size, and distribution width. The particle number density is then calculated from the volume backscatter coefficients. The determination of accuracy with respect to the physical properties of the target suspension requires four or more frequencies to provide comparisons of multiple, independent, 3-frequency solutions representing the same physical acoustic target.

Part 1 illustrates the application of the existence conditions to the elastic sphere backscatter model of Faran (1951), with examples drawn from the only available multi-frequency data set, the 4-frequency Peace River frazil ice measurements of Marko et al. (2015). This establishes that the 3-frequency solutions for the elastic sphere model are not available for this data set; the, less informative, 2-frequency solutions were sufficient to provide estimates of frazil volume concentration. The current paper presents the development of an enhanced empirical scattering model for frazil ice which satisfies the criteria for 3-frequency solutions over the wavenumber range available with current data sets.

2. The semi-empirical pseudo-frazil acoustic backscatter relationship

The improvements in the backscatter cross section model introduced below represent a preliminary attempt to account for the complications intrinsic to suspensions of a population of randomly oriented, disk-shaped, ice particles. Central to the analysis is the assumption that a_e, the radius of an equivalent volume sphere (Ashton, 1983), can be extended to represent the scale length $k_1 a_e$ for a generalized backscatter cross section relationship $\sigma_{BS}(k_1, a_e)$, k_1 being the incident wavenumber. The development draws on two principal sources of information, firstly on the Marko and Topham (2015) laboratory measurements of backscatter cross sections for a family of polystyrene hexagonal disk surrogates, and, secondly, on volume backscatter coefficients derived from frazil data of the Peace River measurements (Marko et al., 2015). The task is addressed by separating the cross section relationship into a longwave Rayleigh component, and the sum of remaining higher order terms. The Rayleigh contribution utilizes the oblate spheroid (Rayleigh, 1897), with the higher order terms deduced from the laboratory disk measurements. The transposition of results derived from the laboratory measurements to the natural frazil environment draws on computational studies of spherical target models. The modern treatment of the elastic sphere algorithm utilized here, and in Part 1, is publicly available as implemented by Dezhang Chu of the Northwest Fisheries Science Center:

(https://github.com/gavinmacauly/calibration-code/tree/master)

To separate the higher order terms, the normalized backscatter cross-section relationship is written in the generic form of Eq. 1, where M and D are the monopole and dipole terms of the Rayleigh solution, and O the sum of higher order contributions

$$\frac{\sigma_{BS}}{\pi a_e^2} = \left[\frac{(k_1 a_e)^2}{3\sqrt{\pi}} (M+D) - \frac{(k_1 a_e)^2}{3\sqrt{\pi}} O \right]^2 \quad , \tag{1}$$

The higher order terms $(k_1 a_e)^2/(3\sqrt{\pi})O$ can then be expressed in terms of known constituents,

$$\left(\frac{(k_1 a_e)^2}{3\sqrt{\pi}} \right) O = \left(\frac{\sigma_{BS}}{\pi a_e^2} \right)_{Ry}^{1/2} - \left(\frac{\sigma_{BS}}{\pi a_e^2} \right)^{1/2} \quad , \tag{2}$$

where the subscript Ry indicates the Rayleigh solution.

2.1 Laboratory measurements on polystyrene disks and spheres

The availability of 0.125 mm thick, precision-cut hexagonal polystyrene disks, with widths ranging from 0.38 mm. to 6.35 mm, (Marko and Topham, 2015), provided measurements of backscatter cross sections for populations of identical surrogate targets with dimensions closely approximately frazil ice particles. A key component of the tests was inclusion of 0.59 mm diameter spherical polystyrene microbeads equal in volume to the 1 mm width disks. Backscatter measurements were made near-simultaneously at four different frequencies (125, 200, 455, and 769 kHz) in neutrally

buoyant brine suspensions. The neutral buoyancy eliminates the dipole term from the longwave Rayleigh contribution, confining the effects particle geometry to the higher order terms.

Complications arose from a shortcoming of polystyrene as a frazil surrogate, in that its characteristic shear wave speed is less than the speed of sound in the host fluid. This allows polystyrene sphere and disk targets to sustain acoustic surface waves which introduce prominent transmission and scattering anomalies (Hay and Schaafsma, 1989; Hefner and Marston, 2000, 2001). These results are excluded from the present investigation, as they are not relevant for ice/freshwater scattering. This limitation restricted the measurements on disk targets to $k_1 a_e$ values ≤ 0.58: roughly the lower half of the $k_1 a_e$ range typical of frazil measurements. In addition, the 125 kHz measurements for both microbeads, and for disks up to 2.4 mm width suffered anomalous elevations of roughly 2 dB relative to the theoretical sphere relationship, subsequently traced to sensitivity at this frequency to disturbances generated by manual concentration sampling (Marko and Topham, 2015). For present purposes, these elevated 125 kHz measurements have also been excluded.

Input values of the polystyrene shear and longitudinal wave speeds for theoretical calculations were slightly adjusted to optimize the agreement between spherical microbead measurements and the corresponding elastic sphere computations. The adjusted wave speeds of 1100 ms^{-1} and 2380 ms^{-1}, differed only by 4% and 2% from corresponding speeds calculated by Hay and Schaafsma (1989) from published elastic constants. The spherical target theory then provides a calibrated reference for the disk measurements which accounts for inter-transducer calibration errors. Estimates of backscattering cross sections were limited to s_V data with linear dependences on concentration. Complete details of underlying measurements and conclusions are provided in Marko and Topham (2015).

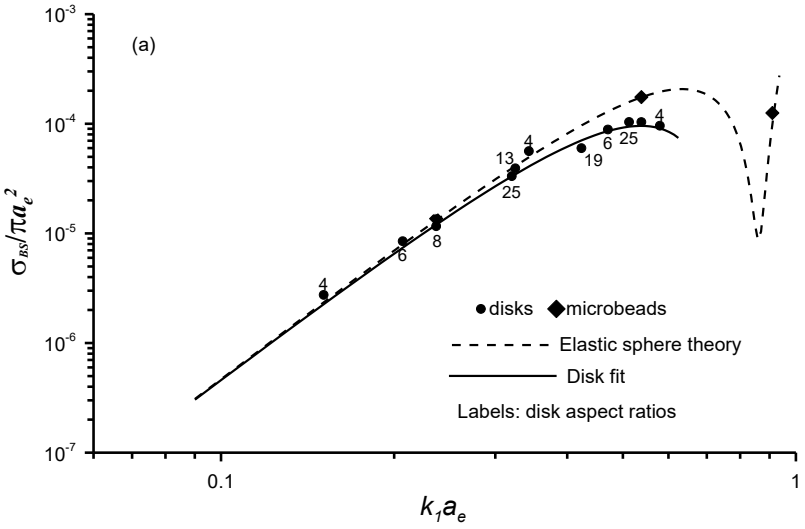

Figure 1a. Summary of single species 1mm polystyrene disks and microbeads, for normalized cross section results a function of $k_1 a_e$. Disk are denoted by circles, microbeads by diamonds.

Figure 1a summarizes the measurements for disk widths up to 3.18 mm, with individual points labelled with the width to thickness aspect ratio, w/t. Apart from a single point with aspect ratio 4 at $k_1a_e = 0.34$, the disk data closely follow the sphere theory up to $k_1a_e \approx 0.3$, followed by a progressively increasing shortfall to about 2.5 dB at the upper disk limit of $k_1a_e = 0.58$. The close collapse of the disk results with the k_1a_e scaling, irrespective of their aspect ratio, supports the extended k_1a_e equivalent sphere scaling assumption.

Differencing the measurements of the equal volume 1 mm (aspect ratio 8) and spherical microbead suspensions eliminates common measurement errors in the acoustic cross sections, including transducer calibrations, and the above-discussed overestimates of 125 kHz cross sections. Subtraction of sphere and disk equations of the form (1), then allows the higher order disk terms to be extracted from the subtracted measured quantities:

$$\left(\frac{(k_1a_e)^2}{3\sqrt{\pi}}\right)(O_D - O_S) = \left[\left(\frac{\sigma_{BS}}{\pi a_e^2}\right)_S^{1/2} - \left(\frac{\sigma_{BS}}{\pi a_e^2}\right)_D^{1/2}\right]_{measured}, \qquad (3)$$

where the subscripts S and D indicate sphere and disk values respectively. The higher order terms of the sphere are derived from computations of the elastic sphere theory, the quantities within the square brackets are individual measured values.

The disk and sphere measurements are compared in Table 1.

Table 1. Comparisons between elastic sphere theory and measured microbead and 1mm disk backscatter cross sections.

Frequency kHz	k_1a_e	$\sigma_{bs}/\pi a_e^2$ Measured microbead	$\sigma_{bs}/\pi a_e^2$ Measured, 1mm disk	$\sigma_{bs}/\pi a_e^2$ Faran theory microbead	Difference microbead-disk
125	0.148	3.394E-06	3.213E-06	2.254E-06	1.82E-07
200	0.237	1.365E-05	1.177E-05	1.353E-05	1.88E-06
455	0.538	1.754E-04	1.025E-04	1.767E-04	7.29E-05

Note the near-equality of the 125kHz microbead and 1 mm disk terms, and their elevation with respect to the theoretical sphere theory, the final column lists their differences. The higher order disk terms O_D obtained from Eqn. (3) are applied to calculate the corresponding backscatter cross-sections for polystyrene disks from Eqn. (1), and listed in Table 2.

Table 2. Backscatter cross-section and higher order terms for polystyrene disks.

k_1a_e	$\sigma_{bs}/\pi a_e^2$ Sphere theory	Higher order disk terms	$\sigma_{bs}/\pi a_e^2$ disk
0.148	2.254E-06	6.094E-05	2.1065E-06
0.237	1.353E-05	4.571E-04	1.1659E-05
0.538	1.767E-04	9.863E-03	1.0353E-04

The higher order disk terms corresponding to Fig. 1a are shown in Fig 1b. The terms listed in Table 2 derived from the differencing are marked by cross symbols, and are well fitted by a simple power law, indicated by the solid line. The circular symbols show the higher order terms of the disk points of Fig. 1a derived directly from Eqn. (2), without the error cancelling conferred by the matched volume differencing. With the exception of the low point at k_1a_e below about 0.3, where differences from the sphere theory are small, the points closely align with the power law fit of the differenced points. The aspect ratio 4 and 13 points at k_1a_e = 0.35, (w = 0.5 mm, 455kHz) correspond to the only significant cross section overestimate. More important is the close correlation of all points above k_1a_e = 0.4, as these confirm and extend the power law to the k_1a_e limit of 0.58. The close correlation irrespective of the aspect ratio confirms the validity of the extended equivalent volume sphere assumption.

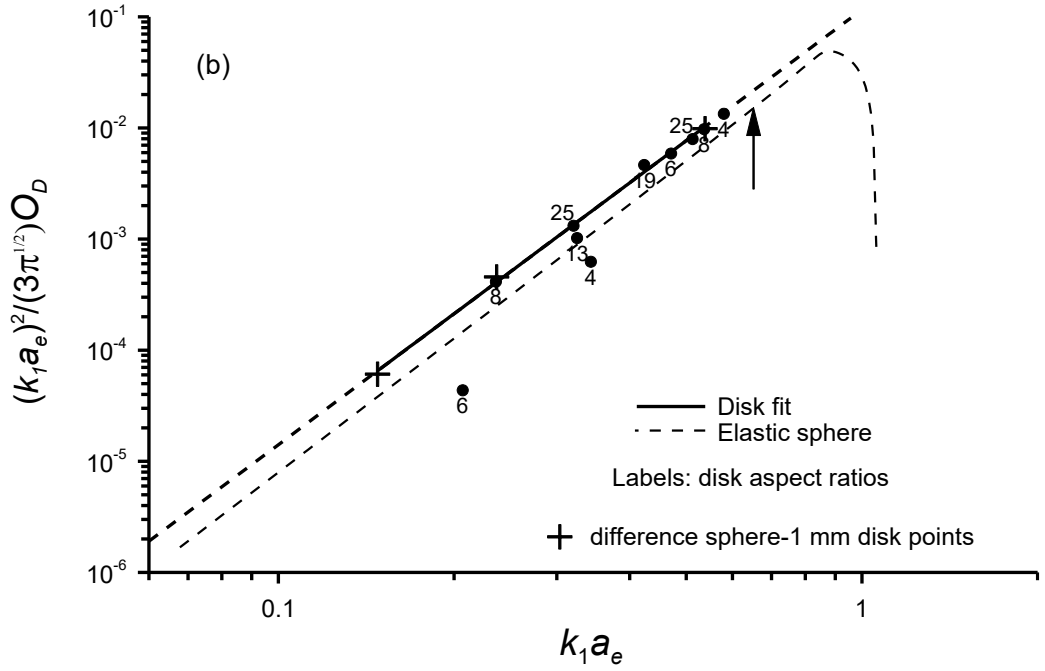

Figure 1b. Higher order terms of polystyrene disks and elastic sphere theory, + differenced measurements, ● individual measurements.

For comparison, the higher order relationship from the elastic sphere theory is also included; this follows a similar power law to the disks for k_1a_e values to approximately 0.8, before reaching a maximum at 0.88. An arrow denotes the maximum in theoretical elastic sphere cross sections at a value well within the power law portion of the higher order term behaviour. This is suggestive of high probabilities for a similar local maximum in the disk cross section relationship. The final form of the reconstructed disk backscatter cross section relationship is representative of a suspension of disks of random orientation and aspect ratios, with the latter quantities ranging between 4 and 25, encompassing the anticipated range of river frazil particle variations.

.

2.2. Transposition of polystyrene disk backscatter results into the river frazil environment.

For applications to frazil ice, the randomly oriented disk backscatter cross section relationship of Fig. 1a must be translated from the neutrally buoyant brine/polystyrene environment to the weakly positive buoyant freshwater/ice environment. This introduces a negative dipole term into the oblate spheroid long wavelength solution (Rayleigh, 1897), which is now sensitive to both aspect ratio and orientation. As the incident wave vector becomes aligned with the radial plane of the oblate spheroid, the negative contribution of dipole decreases, increasing the total backscattered energy.

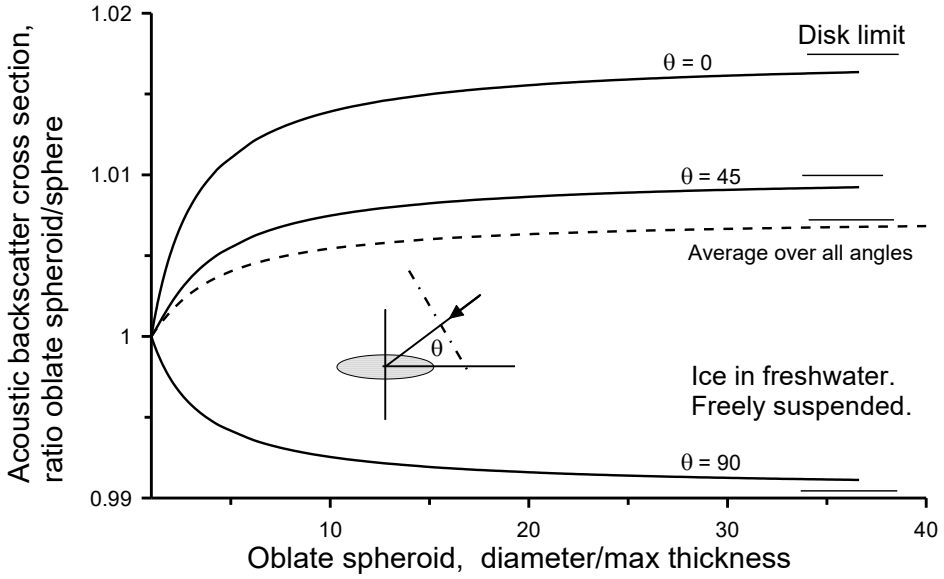

Figure 2. The Rayleigh limit acoustic backscatter cross section as a function of diameter/thickness ratio and orientation for a freely suspended oblate ellipsoid relative to the equivalent volume sphere.

Fig. 2 compares the Rayleigh solution for the backscatter cross section of an oblate spheroid of ice suspended in freshwater with corresponding cross sections of an equivalent volume sphere, where the spheroid is progressively transformed at constant volume from a sphere to the thin disk limit. The insensitivity of the scattering strength to particle shape is evident over the included range of incidence angles. Subsequent averaging over all orientations yields results which are essentially independent of the diameter to thickness ratio, with a maximum deviation from the sphere of 1.0036. Effectively, the Rayleigh solution closely resembles that of the equivalent volume sphere.

The transposition of the higher order terms is more problematical, and for guidance we draw on comparisons of the higher order terms of a selection of sphere models: the brine/polystyrene and freshwater/ice environments for the elastic sphere; and the freshwater/ice environment for the liquid sphere. The normalized theoretical backscatter cross sections, $\sigma_{BS}/\pi a_e^2$, for each of these models are plotted in Fig. 3a as functions of $k_1 a_e$. The elastic sphere cross section curves (A and B) are distinguished by deep local minima in the vicinity of $k_1 a_e = 1$, these vary in depth and width in response to the differences in host fluid and target material properties. These are distinguished

by the ratio of shear wave speeds in the target material to the speed of sound in the host fluid. For polystyrene/brine (A), characterized by the most pronounced minimum, this ratio is less than unity, while for ice/freshwater (C), the ratio exceeds unity, and the depth of the minimum is reduced. The liquid model which cannot sustain shear stress has no minimum. Comparisons with calculations (not shown) for ice spheres in neutral density suspensions showed the effects of small density differences to be largely confined to the dipole term, with negligible effect on the higher order terms. The backscatter characteristic derived from the brine/polystyrene disk suspensions is shown as curve (B),

The corresponding sums of higher order terms deduced from Eqn. 2 are plotted in Fig. 3b; the ordinates of the ice and liquid ice sphere curves are displaced by one and two decades respectively to facilitate visual comparisons. They are remarkably similar, and obey simple power laws over the required range of $k_1 a_e$ (bold solid lines) listed in Table 3. For the two elastic sphere models, the higher order power laws extend beyond the local peaks of the cross-section curves; their corresponding positions are marked by arrows in Fig. 3(b).

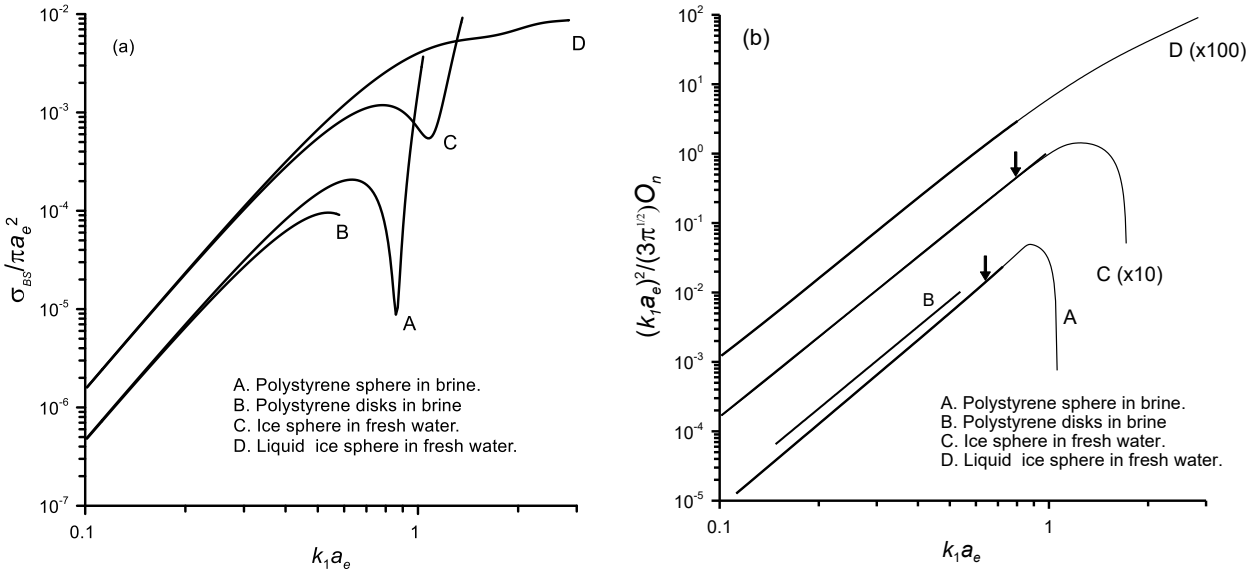

Figure 3. (a) Backscattering cross sections of spherical and disk-shaped polystyrene and spherical ice targets. (b). Higher order terms extracted from the cross sections of (a). Origins of curves C and D are shifted by multiplication by factors of 10 and 100 for clarity: Arrows denote the positions of corresponding peaks in the sphere cross sections of 4 (a).

The major difference between the higher order terms lies in the coefficients of the power law representations, and in lieu of obvious alternatives, it was assumed that the higher order disk terms of natural freshwater frazil bore the same ratio to the ice sphere as the corresponding ratio for the polystyrene/brine system. The parameters of the associated power laws are listed in Table 3 below, the final row listing the values deduced for the frazil ice/freshwater system.

Table 3. Power law fits to higher order backscatter terms, $O.(k_1a_e)^2 /(3\sqrt{\pi})$

Model environment	Coefficient a_0	Power law index m	k_1a_e range	Rayleigh coefficient, R
Polystyrene sphere/brine	0.0836	4.0307	0.11 to 0.9	4.7854E-03
Elastic ice sphere/water	1.0777	3.8234	0.1 to 1.0	1.5591E-02
Liquid "ice" sphere/water	0.0710	3.7769	0.1 to 0.8	1.5591E-02
Polystyrene disk/brine	0.1159	3.9145	0.1 to 0.58	4.7865E-03
Transformed, ice disk/water	1.4940	3.7131	0.1 to 0.657	1.5591E-02

The transformed normalized backscatter cross section relationship is henceforth referred to as the "pseudo-frazil" relationship, and is considered to be validated by the laboratory disk measurements to $k_1a_e = 0.6$.

2.3 Field data extrapolation of laboratory derived disk backscatter cross-sections.

In practice, measurements in natural frazil ice extend beyond $k_1a_e = 1$, and practical applications dictate that the "validated" pseudo-frazil cross section derived from the laboratory measurements be extended to higher k_1a_e values. This step utilized a "bootstrap" technique in which frazil population parameters derived from within the validated region, are used to invert data simultaneously acquired in higher frequency channels. Such an extension provides estimates of σ_{BS} at k_1a_e values beyond the validated regime. Two-channel processing, based on the assumption of a uniform particle distribution, is used to provide estimates of particle number density and equivalent volume radius a_e from within the validated region compatible with the single species laboratory data. Field data to support this effort was selected from 4-frequency Peace River data sets collected during a 2011-12 deployment (Marko et al., 2015). Although data were collected at four frequencies (125, 235, 455 and 774 kHz), erratic features of the 235 kHz data limited options to data acquired in the other three data channels. The March 20 frazil interval, which contained long periods of stable, slowly varying backscatter data, provided a suitable data base for bootstrap extensions.

The long wavelength Rayleigh component of the solution is a known quantity, and the need for empirical extrapolation is thus confined to the higher order terms. The smooth monotonic behaviour over the range of interest, Fig. 3b, provides a relatively robust basis for the extrapolation; the extended cross section relationship is then calculated from Eqn. (2). A 3rd order polynomial provided interpolation between the validated region and the bootstrap points. A corresponding data set from the highly dynamic Jan 14 frazil interval provided an independent check on the bootstrap values. Figure 4a shows the completed extension of the pseudo-frazil higher order terms. The insert shows a detail of the bootstrap region, with the independent set of Jan 14 points merging smoothly with the March 20 bootstrap points. The combined set of points represents a wide range of frazil formation conditions. The corresponding cross section relationship is shown in Fig. 4b. The pseudo-frazil curve differs from the sphere most strongly over the k_1a_e range between 0.6 and

1.0, with a maximum reduction of 4 dB at $k_1 a_e$ = 0.8, a critical operational range for river ice studies.

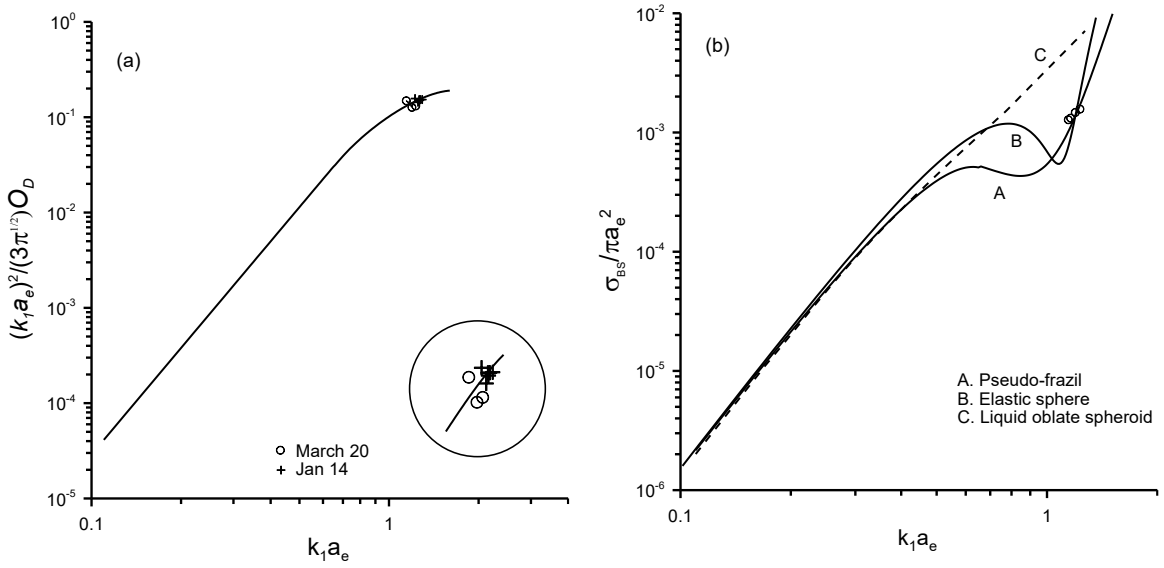

Figure 4. (a) Pseudo-frazil bootstrap extrapolated higher order fit. (b) Normalized backscatter cross sections characteristics of the pseudo-frazil (A), elastic sphere (B), and a randomly oriented liquid 30:1 aspect ratio oblate spheroid (C).

The freshwater pseudo-frazil relationship (A) is given by:

$$k_1 a_e \leq 0.657: \quad \frac{\sigma_{BS}}{\pi {a_e}^2} = \left[R^{1/2}(k_1 a_e)^2 - a_0 (k_1 a_e)^m\right]^2, \tag{4}$$

$$k_1 a_e > 0.657: \quad \frac{\sigma_{BS}}{\pi {a_e}^2} = \left[R^{1/2}(k_1 a_e)^2 - (b_0 + b_1(k_1 a_e) + b_2(k_1 a_e)^2 + b_3(k_1 a_e)^3)\right]^2,$$

R = 0.015591, a_0 = 1.4948, m = 3.7131, b_0 = 0.005234, b_1 = -0.1635, b_2 = 0.4022, b_3 = -0.1424.

The solution maps defining the conditions necessary for a data set to sustain complete 3-frequency solutions are shown in Figs 5a and 5b, for the March 20 and Jan.14 frazil intervals respectively. They are presented in terms of the ratios of non-logarithmic volume backscatter coefficients s_{Vi}/s_{Vj} expressed as *G(i,j),* where *i* and *j* specify data channel numbers. The parameter *b* is the width of the lognormal particle distribution. For solutions to exist, the data points must lie above the lower boundary of the diagram, a condition satisfied by a high proportion of both the March 20 and Jan 14 data sets. These are representative of the extremes of 2011-12 winter freeze up conditions. It is important to note that the solution map determines not only the existence of solutions prior to analysis, but also the individual particle distribution widths, a feature which provides guidance in selecting data suitable for 2-channel analysis.

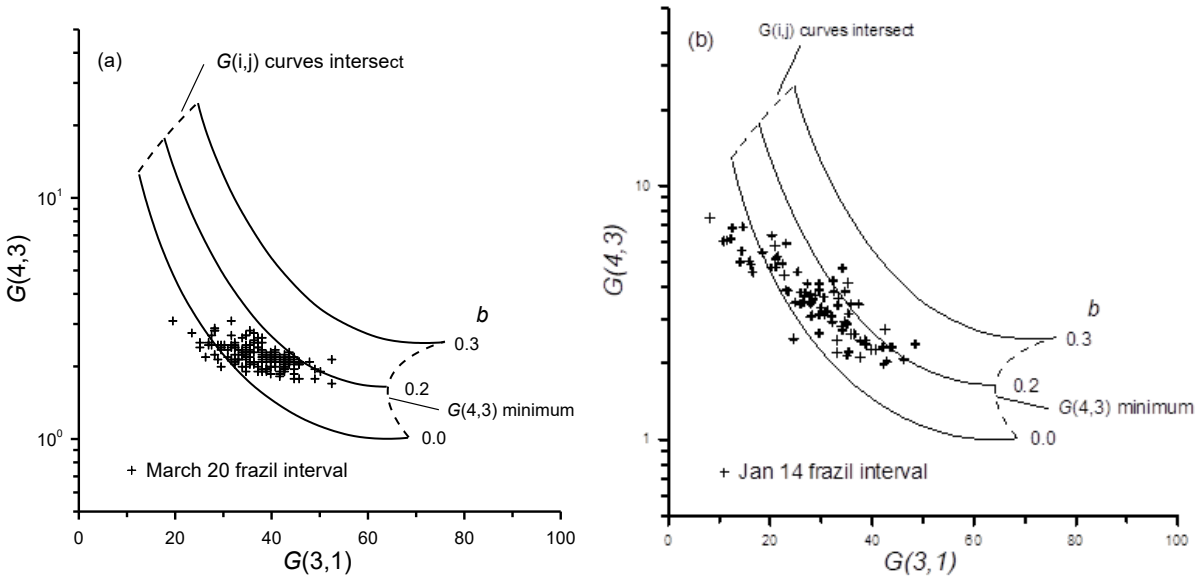

Figure 5. Pseudo-frazil 3-frequency solution diagrams; (a) the March 20 frazil interval, (b) Jan 14.

The 3-frequency solutions are illustrated in Fig. 6a for frazil fractional volume, F(t), at an elevation of 2.6 m. during the March 20 frazil interval. These solutions are compared with the weighted mean of the three, 2-channel solutions, available for the elastic sphere model. The F(t) scale of the latter has been adjusted by a factor of 0.5 for the optimal visual comparison with the 3-frequency pseudo-frazil results. Figure 6b shows the corresponding distribution of the pseudo-frazil distribution widths. These values of b result in a roughly 10% underestimate of fractional volumes computed from the combined mean of 2-frequency solutions, compared with 3-frequency solutions.

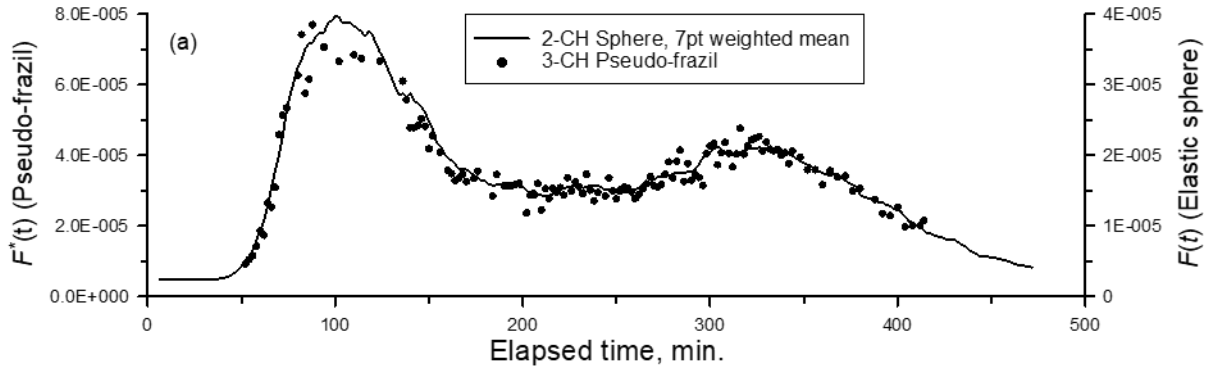

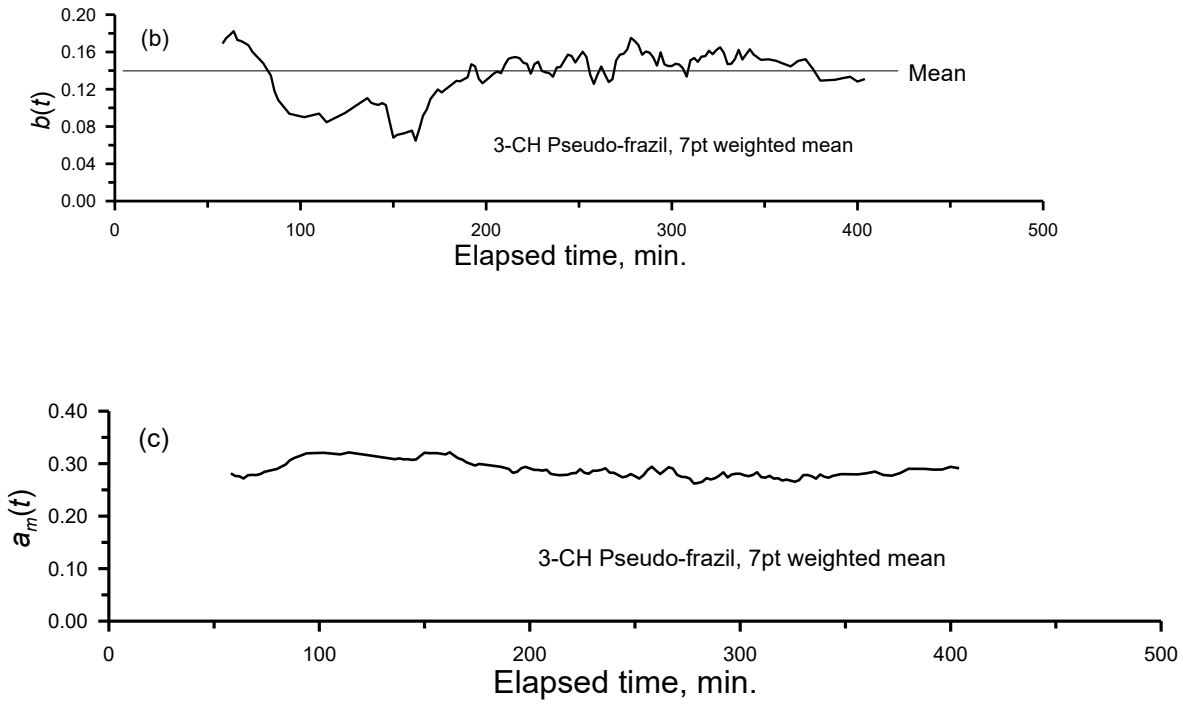

Figure 6. March 20 frazil interval, fractional volume *F(*t) at 2.6 m. elevation: (a) 3-channel pseudo-frazil model solutions ●; ─ elastic sphere model solutions, 7 pt. weighted mean of three, 2-channel combinations, note 2:1 difference in vertical scales. (b) Pseudo-frazil particle distribution widths, 7 pt. weighted mean. (c) Pseudo-frazil mean equivalent volume sphere radius a_m(t), 7 pt. weighted mean.

The range of the bootstrap extrapolation of the pseudo-frazil model is limited by the narrow range of a_e values available from the river frazil data, and, accordingly, represents only as a first step in the development of the backscatter model. As presented, here, it demonstrates the utility of the "bootstrap" technique, and provides full 3-channel solutions for a high proportion of currently available data sets.

3.0 Evaluation of an alternative frazil characterization utilizing the pseudo-frazil model

An alternative approach to frazil acoustic analysis has been applied to characterizations of Antarctic ice shelf plume by Frazer et al.(2020). It is based upon the 30:1 aspect ratio liquid oblate spheroid developed by Kungl et al. (2020) which was judged to be more representative of frazil ice than the equivalent volume sphere approach. To facilitate comparison with the elastic sphere and the pseudo-frazil relationships, the Kungl relationship has been re-scaled, replacing the original diameter-based scaling by the effective sphere radius a_e. To account for the change from sea to freshwater, the overall magnitude has been adjusted to match low $k_1 a_e$ values to the Rayleigh solution of the pseudo-frazil relationship Fig. 4b, curve C. The liquid spheroid relationship resembles the liquid sphere, Fig 3a, departing strongly from both elastic sphere, and semi-

empirical pseudo-frazil relationships for $k_I a_e$ values above 0.4: behaviour attributed to the absence of shear stress in liquid models.

Comparison of the results are complicated by the fact that the bulk of the Frazer et al. results are presented as colour-coded images. The exception was a single figure presenting plots of median S_V values recorded by the upward looking sonar at frequencies of 125, 200, 455 and 769 kHz for depths between 10 and 35 mBSL over a single 11 minute interval centered on 17:59, Nov. 11, 2017. This provided an opportunity to apply the pseudo-frazil relationship to validate a full 4-frequency independent data set with frequencies almost identical to those used in the Marko et al. (2015) Peace River deployment. The digitized S_V values provided representative data at depths of 10 mBSL and at 15mBSL, the reference level chosen by Frazer et al. as a focal point in their discussions. Unfortunately, text on the Frazer et al. Figure obscured the channel 1 S_V values for this level, reducing the 15 m evaluation from four to three frequencies. The digitized data are listed in Table 4 below, and are uniformly about 20 dB below S_V data acquired at similar frequencies, and corresponding to the peak Peace River fractional volume results of Fig 6.

Table 4. The digitized Frazer et al. volume backscatter coefficients at 10 and 15 m.

Dept, mBSL	S_V1, dB	S_V2, dB	S_V3, dB	S_V4, dB
10	-74.3	-69.3	-61.9	-57.4
15	-	-73.6	-66.4	-61.5

The four channel data provides six 2-frequencyand four 3-frequency independent solutions for inter-comparison, and the reduced 15 m data allow three independent 2-frequency solutions and one 3-frequency solution. The fully pseudo-frazil processed data set is presented in Table 5 below.

Table 5. Two- and three-channel extraction results obtained by applications of the pseudo-frazil cross section-based processing algorithm to the Frazer et al. (2020) 10 and 15 m S_V data.

Depth (mBSL)	Channel pair	a_m (m)	b	N^*	F^*, F	F^*_{Ave}, excluding (2,1) pair	$(F^*-F^*_{Ave})/F^*_{Ave}$
10	(2,1)	0.59	-	576	5.07E-07	1.43E-06	-0.65
10	(3,1)	0.36	-	7945	1.67E-06		0.17
10	(3,2)	0.33	-	8804.	1.39E-06		-0.03
10	(4,3)	0.34	-	8512	1.48E-06		0.02
10	(4,2)	0.35	-	6498.	1.21E-06		-0.15
10	(4,1)	-	-	-	-		
10	(2,1)(3,2)	0.49	0.18	1013	5.89E-07		
10	(4,3)(3,2)	0.32	0.10	9638.	1.40E-06		
10	(4,1)(4,3)	-	-	-	-		
15	(3,2)	0.34	0.00	3104	5.027E-07	4.89E-07	0.027
15	(4,2)	0.36	0.00	2119	4.255E-07		-0.130
15	(4,3)	0.35	0.00	2992	5.395E-07		0.103
15	(3,2)(4,3)	0.32	0.12	8512	5.041E-07	5.04E-07	

A notable feature is the pattern of anomalous 10 m results obtained with combinations containing channel 1. For example the F^* and F values for (2,1) and (1,2, 3) combinations fall short of other two channel results by more than 50%. The (4,1), (1,2,4),(1,3,4) combinations also failed support solutions, with the (4,1) data falling below the *G(4,1)* relationship. These results suggest that the channel 1 S_V value data were elevated, possibly by background noise, given the low signal levels. Neglecting the anomalous (2,1) extraction, the two channel mean and uncertainty can be expressed as $F^* = 1.4 \times 10^{-6} \pm 2 \times 10^{-7}$, equal to the (4,3)(3,2) F value for $b = 0.1$. The low value of b satisfies the narrow distribution requirement for representative values of F^*. The mean F^* is roughly 20 dB below the maximum Peace River fractional volume estimates of Fig 6a which is in accord with observed differences in corresponding S_V values. The general pattern of behaviour of the 15 m data closely parallels the 10 m results, but with reduced fractional volumes of $F^* = 4.9 \times 10^{-7}$ and $F = 5.0 \times 10^{-7}$, about 12dB below the Frazer et al. estimate of 8×10^{-6}.

The unusually skewed and broadened nature of the lognormal distribution of frazil disk diameters derived by Frazer et al. corresponds a distribution width parameter $b = 1.3$, an order of magnitude above the river estimates in Fig 6b, and as measured by McFarlane et al., (2017). The accompanying particle number densities of 3×10^3 m^{-3} represents, on average, 3 frazil disks per litre of water; a level undetectable in the Marko and Topham (2015) laboratory tests. The alarming level of disagreement between the Frazer et al. analyses and our own, raises serious doubts as to the utility of the Kungl spheroid, and merits further investigation. A search for simple 2-frequency solutions within the Kungl framework provided the least restrictive form of evaluation. The evaluation is presented graphically in Figures 7a and b comparing the Kungl s_V ratios *G(i,j)* as functions of the effective radius a_e, alongside corresponding measured quantity ratios for the 4–frequency data of Frazer et al. as indicated by the vertical extent of the labelled symbols.

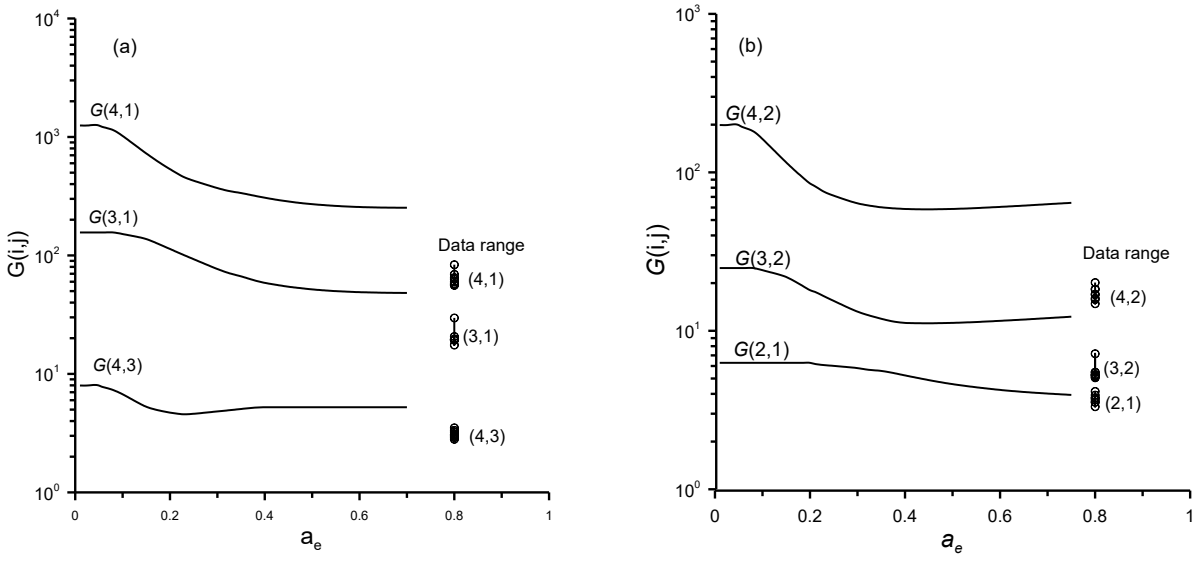

Figure 7. Two channel ratio functions for the liquid oblate spheroid (Kungl et al., 2021); a) channel ratios (3,1), (4,3) and (4,1); b) ratios (3,2), (4,2) and (2,1). Symbols indicate the range of corresponding Frazer et al (2020) s_V data ratios for depths between 8 m. and 18 m.

It can be seen that, with the exception of a single (2,1) point, the data ratios fail to intersect corresponding theoretical ratio functions and 2-frequency solutions cannot exist. As such solutions are fundamental, their existence is essential for obtaining more informative 3-frequency solutions. As a matter of interest, the exceptional (2,1) point yielded a sum total of 83, 2mm diameter, 30:1 aspect ratio particles per cubic metre, a fractional volume of 3×10^{-13}. The number density is in line with the Frazer et al. analysis, but is combined with ultra-low fractional volumes, consistent with the low S_V data and the steeply rising backscatter relationship of the Kungl spheroid. This and the otherwise complete absence of solutions raises concerns over the method of analysis employed by Frazer et al., which relied on the optimization of a simultaneous 4-frequency search algorithm for the unknown parameters (μ, σ and N). These "optimizations" stand in strong contrast to the numerically precise 3-frequency solutions utilized for the pseudo-frazil analysis.

The credible results obtained from the pseudo-frazil analysis and its validation, indicates that the small sample of data provided by Fazer et al. is of sufficient quality to encourage further consideration of the Antarctic data set along the lines suggested by Marko and Topham (in preparation).

4.0 Summary and conclusions

A semi-empirical backscatter cross section relationship has been developed to describe a suspension of randomly oriented frazil ice crystals of varying aspect ratio. The formulation is based on an extension of the equivalent volume- or effective-sphere assumption of Ashton (1983) which allows use of a general cross section relationship, $\sigma_{BS}\ (k_1,\ a_e)$ for quantitative characterization of frazil populations from backscattering data. This cross section is a sum of two components consisting of the longwave Rayleigh solution for a freely suspended oblate spheroid and the sum of higher order terms deduced from 4-frequency acoustic laboratory measurements on suspended neutrally buoyant polystyrene spheres and disks. The fixed thickness disks closely matched the geometry of natural frazil ice crystals. The backscatter cross section measurements collapsed to a well correlated $\sigma_{BS}\ (k_1 a_e)$ relationship, irrespective of aspect ratio, confirming the validity of the extended equivalent volume sphere scaling. The availability of data on polystyrene spheres with volumes identical to those of tested 1 mm disk species, provided direct measures of shape effects at common $k_1 a_e$ values. Differencing then eliminated common measurement errors, and facilitating the extraction of the higher order terms valid for $k_1 a_e$ values up to 0.58. The resulting cross section relationship for polystyrene/ brine suspension offers a quantitative description of the key physical characteristics of suspensions of randomly oriented, thin elastic flat disks such as frazil.

The transfer of the polystyrene/brine relationship into the freshwater frazil environment utilized the strong similarity of the higher order terms to those of equivalent elastic spheres in both environments. Within the $k_1 a_e$ range of interest, all exhibit similar power law dependences and it was assumed that the higher order terms of natural frazil ice were related to their equivalent elastic sphere counterparts by the ratio linking the higher order polystyrene disk- terms those of the equivalent polystyrene sphere. The transferred relationship was then extrapolated to a $k_1 a_e$ value

of 1.2 by a "bootstrap" technique utilizing the high frequency channel of the Peace River data. The final relationship, denoted the "pseudo-frazil" backscatter model, is capable of returning exact 3-frequency solutions for a 2-parameter lognormal particle distribution for both river and marine frazil ice data.

When conditions for solution existence are satisfied, the equations are solved in terms of ratios of measured volume backscatter coefficients (Hay and Sheng, 1992), a technique which eliminates particle number density from a two parameter search routine which rapidly converges to an exact solution. The particle number density then is calculated directly from the volume backscatter coefficients. When more that three frequencies are available, multiple sets of backscatter ratios yield independent solutions which provide a measure of the quality of the match between backscatter model and the data.

The pseudo-frazil model derives estimates of frazil fractional volume from 2- and 3-frequency data with uncertainty of about 20%, sufficient for many practical purposes. The present version is limited in range by the currently limited availability of field data due, in part, to the unreliability of data collected at 235 kHz in the 2011-2012 Peace River study (Marko et al., 2015). Access to data at this frequency and/or additional field measurements can further refine the pseudo-frazil cross section relationship and, in particular, extend it to higher $k_l a_e$ values. More innovative approaches to obtaining a more perfect extraction algorithm may be possible but should be guided by compatibility with the two-channel testing procedures which underlie the pseudo-frazil approach. In our opinion, liquid target-based algorithms are unlikely to be productive in this respect as they cannot reproduce the complicated parameter dependences characteristic of scattering by elastic solid targets.

References

Ashton, G. D., 1983: Frazil ice. In: Theory of Dispersed Multiphase Flow, Academic Press N.Y., 271-289.

Chu, D., Northwest Fisheries Science Center. https://github.com/gavinmacauly/calibration-code/tree/master.

Faran, J.J. Jr., 1951: Sound scattering by solid cylinders and spheres. J. Acoust. Soc. 23, pp 405-418.

Frazer, E. K., Langhorne, P. J, Leonard, G. H., Robinson, N.J. and Dániel Schumayer, D. Observations of the size distribution of frazil ice in an ice shelf water plume., 2020. Geophy. Res. Letters, 47, e2020GL090498, https://doi.org/10.1029/2020GL09049.

Hay, A. E, and Sheng, J. 1992: Vertical profiles of suspended sand concentrations and size from multifrequency acoustic backscatter. J. Geophys. Res. 97 (10), pp 1566-1567.

Kungl, A. F., Schumayer, D., Eamon K. Frazer, A. K., Pat J. Langhorn, P. J., Greg, H., Leonard, G. H., 2020: An oblate spheroidal model for multi-frequency acoustic back-scattering of frazil ice. Cold Reg. Sci Technol, 177, https://doi.org/10.1016/103122.

Marko, J. R., Topham, D.R. (2015):Laboratory measurements of acoustic backscattering from polystyrene pseudo- ice particles as a basis for quantitative frazil characterization. *Cold Reg. Sci. Technol. 112*, 66-86.

Marko, J.R., Jasek, M., Topham, D.R., 2015: Multifrequency Analyses of 2011-2012 Peace River SWIPS frazil backscattering data. Cold Reg. Sci. Technol. 110, 102-119.

Marko, J.R., and D,R Topham: Comments on "Observations of the size of frazil ice in an ice shelf water plume, (Frazer et al., 2020)". In preparation.

McFarlane, V., Loewen, M., Hicks, F., 2017: Measurements of the size distributions of frazil ice particles in three Alberta rivers. Cold Reg. Sci. Technol. 142, pp. 100-117,

Rayleigh, J.W.S.: On the incidence of aerial and electric waves upon small obstacles in the form of ellipsoids or elliptic cylinders and the passage of electric waves through a circular aperture in a conducting screen. Phil. Mag. (5) XLIV, pp28-52. (Scientific Papers volume 4, p 305. Cambridge Library Collections, 1897).

Topham, D.R., The interpretation of multi-frequency acoustic profiling; Part 1, Exact solutions and their role in the evaluation of acoustic backscatter models, (in preparation).